SMAP RADIOMETER RFI PREDICTION WITH DEEP LEARNING USING ANTENNA COUNTS

A. M. Alam[(1)], *A. C. Gurbuz*[(1)], *M. Kurum*[(1)]

[(1)] Mississippi State University, Mississippi State, MS, USA

ABSTRACT

Soil Moisture Active Passive (SMAP) is a NASA's earth observing satellite which is used for global scale soil moisture measurement and differentiating frozen/thawed state. It is employed in 1400-1427 MHz protected band which uses L-Band radiometer for the quantification. But increasing number of wireless equipment such as air surveillance radar signals and 5G communication are making it harder to protect the radiometer microwave sensing in this secured spectrum. These technologies are responsible for the Radio Frequency Interference (RFI) in SMAP's passive observation. In this study, a novel deep learning architecture is developed that uses convolutional neural network (CNN) to predict RFI. Our model uses SMAP's level 1A raw antenna counts as well as level 1B quality flags to dynamically label these antenna raw measurements as RFI contaminated and RFI free footprints. This example study shows around 94% accuracy in detecting RFI and such result may recommend a lucrative technique in detecting RFI.

***Index Terms*—** SMAP, RFI, Deep Learning, Radiometer

1. INTRODUCTION

RFI has become a matter of concern in earth observation satellites. RFI can jeopardize the received signals and produce faulty values which may prove very harmful. Soil moisture information is critical for anticipating agricultural yield through irrigation planning, which in turn aids in global food production planning. Considering the harmfulness of RFI, SMAP is one of the first satellites to deploy with a data processing unit dedicated to RFI detection and mitigation [1, 2].

There are different types of characterization available for the radiometer RFI. Two observed RFI types for SMAP were pulsed RFI and continuous wave (CW) RFI [3]. RFI can be generated from a single source or multiple sources. There are also low and high level RFI which can be very detrimental in final product calibration. There can be multiple approaches that are modeled for RFI detection. For SMAP, those techniques can be categorized as cross-frequency detection, polarization detection, pulse detection and kurtosis detection. Among these methods, pulsed RFI are detected by pulse and kurtosis detection [4]. On the other hand, CW RFI are detected by cross-frequency detection. All of these techniques are combined to determine whether a footprint contains RFI. Moreover, these RFI detection methods heavily rely on the handcrafted algorithms which needs developing a hypothesis with presumed postulation.

In this paper, a deep learning (DL) approach is proposed which will rely on end-to-end data to decide whether a footprint measurement is RFI contaminated or not. This provides a new perspective where a single algorithm can be utilized to detect RFI. DL, which is a subset of machine learning (ML), proves its stature in different classification and regression-based problems. Traditional RFI mitigation techniques use statistical approaches, which need hypothesis building with a variety of assumptions. But in the DL approach, data is used directly in the model so that the model can learn the most important features directly from the data and be a deciding factor in terms of making decisions. DL is very flexible compared to the traditional approaches and helps to provide a generalization over a certain region. According to author's knowledge, there has been only one study on SMAP's radiometer RFI detection with DL. For example in [5], authors have introduced RFI detection with DL with 5014 spectrogram images for training and validation that used manual inspection for labeling RFI contaminated pixels. Also, the authors of that article used pre-trained DL architectures on spectrogram RGB images with the help of transfer learning to evaluate model's performance in terms of accuracy. In this study, a novel DL architecture is developed which examines 200,000 samples over Europe to detect RFI. This DL architecture helps to tackle the limits of transfer learning [6]. Normalized raw antenna moments are used, which are SMAP level 1A data products and dynamically label them with SMAP level 1B data quality flags. These normalized antenna counts are converted into spectrograms and fed directly into the detection model without converting into the RGB images. These help to preserve the dynamic range of inputs and extract important information related to RFI. Moreover, limited sample sizes with real-world data tend to curb the generalization in classification problems [7]. This study's large sample size helps with the generalization of the DL approach.

Remainder of the paper is organized as follows: Data description is detailed in Section 2, while methodology for RFI

This work was supported by National Science Foundation under Grant No. 2030291 and 2047771.

detection is described in Section 3. Results and discussions are provided on 4 and finally conclusions are drawn in Section 5.

2. DATA DESCRIPTION

In this section, dataset acquisition and development for input to train and test the DL model are discussed. Initial processing stages to prepare data to feed into DL model are provided.

2.1. Data Acquisition

In this study, SMAP level 1A [8] and level 1B [9] data products are utilized. Level 1A data product contains antenna counts which are divided into different sub-band level raw moments. These are the first, second, third and fourth order moments. From these moments data, with the help of complex correlation, SMAP level 1A develops Stokes parameters [10]. In this study, third and fourth Stokes parameters are used as inputs to the DL model. Level 1B data products contain antenna brightness temperature along with 16-bit quality flags. These flags contain a single bit of information that demonstrates whether a footprint is RFI contaminated or not. Antenna count spectrograms are dynamically labeled for training and testing in DL architecture with the help of quality flags which are taken as the ground truth of this study. These level 1A and level 1B data products are collected from a time period of 31 March 2016 to 4 June 2016.

2.2. Data Preparation

For RFI detection, the antenna counts data products are further divided into sub-band levels. For SMAP, RFI signals are received in both sub-band and full band levels. For sub-band, high-resolution signals are categorized in 16 segments where each band consists of 1.5 MHz of the whole allotted spectrum. For each of these sub-bands, there are 8 radiometer science data packets. These data packets are integrated over 1.2 ms. With help of these high-resolution data, spectrograms of antenna counts are developed. Each sample contains an array of $16\ (1.5\text{MHz}) \times 8\ (1.2\text{ms})$ spectrogram. By using third and fourth Stokes parameters we generated approximately 200,000 samples over the Europe region and dynamically label them with level 1B quality flags.

2.3. RFI Characterization

In this part, the spectrograms of the third and fourth Stokes parameters of the antenna counts are demonstrated. These Stokes parameters are generated from the raw antenna moments and to have homogeneity throughout the study, the max-min normalization technique is used. This normalization helps to utilize a single DL architecture for all types of antenna counts [11]. Example spectrogram images are created from third and fourth Stokes parameters can be observed in Fig. 1. Different types of RFI cases as well as RFI free spectogram examples are seen from the figure.

3. METHODOLOGY

Detecting RFI is a difficult task, because of the very little knowledge about its sources. Moreover, there are high and

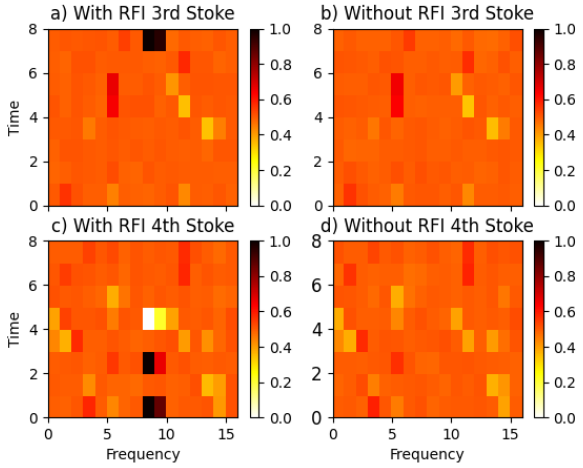

Fig. 1: Spectrogram images generated from third and fourth Stokes parameters from RFI free and RFI contaminated footprints

low-level RFI which can be embedded with signals of interest. So, in this study, a DL architecture with convolutional layers is developed for RFI detection, which will learn directly from SMAP-generated data. A convolutional neural network (CNN) is one of the most popular tools in image classification and is utilized here to detect RFI as a binary classification problem.

This study's DL model has four convolutional layers stacked up one after another. The input to the DL architecture are spectrogram images, hence the image sizes are 16×8. The first layer starts with 16 filters and the number of filters for the subsequent layers are 32, 64 and 128 respectively. Each CNN layer is followed by a Rectified Linear Unit (ReLU) activation function. After extracting features from all the CNN layers, a fully connected layer with 128 neurons is used, which is followed by a dense layer with 2 neurons to feed into the soft-max activation function. The soft-max layer provides a probability of whether a footprint is RFI contaminated or not.

In an DL-based classification, it is important to implement a cross-validation approach to evaluate the performance of a model in a diverse scenario. This technique is indispensable to see the generalization capability of the model. It is a common scenario in ML that the model performs well in training but fails largely when it is tested on unseen data. The final model is designed to make sure that the DL model does not underfit or overfit the training data. To evaluate the model, a train-test split technique is utilized where 80% of the data is randomly kept for training and 20% data for testing. The model is trained with 60 epochs and 128 batch sizes. Receiving operating characteristics (ROC) and confusion matrix are generated to evaluate the detection model with two different datasets such as third and fourth Stokes parameters. Python

and tensorflow keras API is used to build the detection framework. From the confusion matrix, performance metrics such as accuracy, precision, recall and f1-score are generated that are given as

$$Accuracy = \frac{TP + TN}{TP + TN + FP + FN} \tag{1}$$

$$Precision = \frac{TP}{TP + FP} \tag{2}$$

$$Recall = \frac{TP}{TP + FN} \tag{3}$$

$$F1 = \frac{2 * Precision * Recall}{Precision + Recall} \tag{4}$$

where TP = True Positive, TN = True Negative, FP = False Positive and FN = False Negative. Accuracy aids in understanding the model's overall performance. However, high accuracy does not always reflect the performance of each class ("RFI" and "no RFI" in our case), and metrics like precision and recall can help explain performance in terms of false-positive and false-negative detection, which is crucial in RFI detection.

Table 1: Confusion Matrix of RFI Prediction

Antenna Counts Domain	Confusion Matrix (%)			
Third Stokes	True Class	RFI	90.25	9.75
		No RFI	2.5	97.5
Fourth Stokes	True Class	RFI	89.7	10.3
		No RFI	3	97
			RFI	No RFI
			Prediction Class	

Table 2: Evaluation Metrics (%) of RFI Detection Over Europe

Antenna Counts Domain	Accuracy	Precision	Recall	F1-Score
Third Stokes	93.88	90.25	97.30	93.64
Fourth Stokes	93.7	89.7	96.76	93.10

4. RESULTS AND DISCUSSION

In this section, the results of RFI detection with the proposed DL architecture by the train-test split technique are shown. From Table 1, the confusion matrix of the prediction results over the test data can be seen. For third Stokes parameters, the model correctly predicts RFI contaminated pixels 90.25% of the time. Meanwhile, for no RFI cases, DL predicts correctly on 97.5% of the cases. For the fourth Stokes parameter,

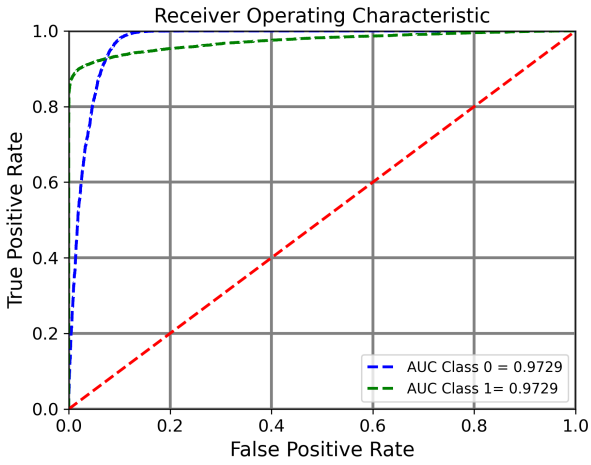

Fig. 2: ROC of RFI prediction with third Stokes parameter - class 0 denotes cases with No RFI and class 1 denotes cases with RFI

RFI detection percentage is 89.7% and the No RFI detection percentage is 97%. Table 2 shows the accuracy, precision, recall and f1 scores of each input. For the third Stokes parameter, accuracy and precision are 93.8% and 90.25% respectively along with a significantly high recall. This depicts the model can anticipate RFI cases which are actually RFI with a relatively low false alarm rate. Moreover, fourth Stokes parameter's accuracy and precision are 93.7% and 89.7% with a high recall performance. These performance metrics with two different datasets help to portray the superiority of DL

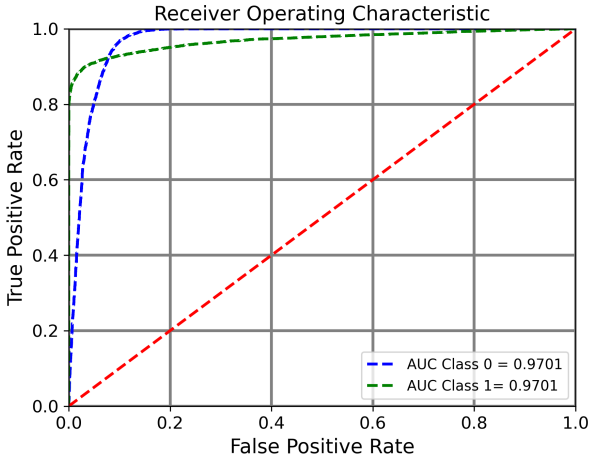

Fig. 3: ROC of RFI prediction with fourth Stokes parameter - class 0 denotes cases with No RFI and class 1 denotes cases with RFI

architecture in detecting RFI.

Fig. 2 illustrates the ROC of RFI detection for the third Stokes parameter. The area under the curve (AUC) in this case is 0.9729 for both of the classes. A higher AUC proves the effectiveness of the detection algorithm under diverse scenarios. ROC shows how the proposed model performs in terms of probability of detection (PD) with respect to the probability of false alarm (PFA) and this study's model provides a high PD while satisfying a low PFA. From Fig. 3, the ROC for the fourth Stokes parameters can be seen. AUC for this prediction is 0.9701. Moreover, traditional approaches for SMAP RFI discussed in [12], show the highest AUC of 0.85 with sub-band kurtosis algorithm. DL model shows enhanced RFI detection performance compared with the traditional statistical approaches.

5. CONCLUSION

In this paper, a novel DL architecture is developed utilizing CNN to detect radiometer RFI in SMAP data. RFI has become a matter of concern with the increasing number of active wireless technologies. We utilized SMAP's level 1A and level 1B data products and build a DL based detection model. The model uses approximately 200,000 spectrogram images as its input. We evaluated the performance of the model using data over the Europe region. Performance metrics are provided in terms of accuracy, precision, recall and f1 scores using a train-test validation technique. Moreover, receiver operating characteristic curves are depicted to provide a perspective in terms of probability of detection and probability of false alarm. This study's model demonstrates approximately 94% accuracy using the third and fourth Stokes parameters.

For future work, we plan to develop RFI detection schemes based on DL architectures taking advantage of varying levels of SMAP data jointly. In addition, we plan to extend provided results to develop a DL based RFI detector to predict the global scale RFI footprints.

6. REFERENCES

[1] D. Entekhabi, E. G. Njoku, P. E. O'Neill, K. H. Kellogg, W. T. Crow, W. N. Edelstein, J. K. Entin, S. D. Goodman, T. J. Jackson, J. Johnson, J. Kimball, J. R. Piepmeier, R. D. Koster, N. Martin, K. C. McDonald, M. Moghaddam, S. Moran, R. Reichle, J. C. Shi, M. W. Spencer, S. W. Thurman, L. Tsang, and J. V. Zyl, "The soil moisture active passive (smap) mission," *Proceedings of the IEEE*, vol. 98, pp. 704–716, 2010.

[2] S. W. Ellingson, G. A. Hampson, and J. T. Johnson, "Characterization of l-band rfi and implications for mitigation techniques," *International Geoscience and Remote Sensing Symposium (IGARSS)*, vol. 3, pp. 1745–1747, 2003.

[3] N. Majurec, J. Park, N. Niamsuwan, M. Frankford, and J. T. Johnson, "Airborne l-band rfi observations in the smapvex08 campaign with the l-band interference suppressing radiometer," *International Geoscience and Remote Sensing Symposium (IGARSS)*, vol. 2, 2009.

[4] P. N. Mohammed, M. Aksoy, J. R. Piepmeier, J. T. Johnson, and A. Bringer, "Smap l-band microwave radiometer: Rfi mitigation prelaunch analysis and first year on-orbit observations," *IEEE Transactions on Geoscience and Remote Sensing*, vol. 54, pp. 6035–6047, 10 2016.

[5] P. N. Mohammed and J. R. Piepmeier, "Microwave radiometer rfi detection using deep learning," *IEEE Journal of Selected Topics in Applied Earth Observations and Remote Sensing*, vol. 14, pp. 6398–6405, 2021.

[6] J. Williams, A. Tadesse, T. Sam, H. Sun, and G. D. Montañez, "Limits of transfer learning," *Lecture Notes in Computer Science (including subseries Lecture Notes in Artificial Intelligence and Lecture Notes in Bioinformatics)*, vol. 12566 LNCS, pp. 382–393, 6 2020.

[7] S. Shahinfar, P. Meek, and G. Falzon, ""how many images do i need?" understanding how sample size per class affects deep learning model performance metrics for balanced designs in autonomous wildlife monitoring," *Ecological Informatics*, vol. 57, pp. 101085, 5 2020.

[8] E. J. Kim P. Mohammed J. Peng Piepmeier, J. R. and C. Ruf., "Smap l1a radiometer time-ordered parsed telemetry, version 2 | national snow and ice data center," `https://nsidc.org/data/SPL1AP/versions/2`, 2015.

[9] P. Mohammed J. Peng E. J. Kim G. De Amici J. Chaubell Piepmeier, J. R. and C. Ruf., "Smap l1b radiometer half-orbit time-ordered brightness temperatures, version 5 | national snow and ice data center," `https://nsidc.org/data/SPL1BTB/versions/5`, 2020.

[10] J. R. Piepmeier, D. G. Long, and E. G. Njoku, "Stokes antenna temperatures," *IEEE Transactions on Geoscience and Remote Sensing*, vol. 46, pp. 516–527, 2 2008.

[11] D. Singh and B. Singh, "Investigating the impact of data normalization on classification performance," *Applied Soft Computing*, vol. 97, pp. 105524, 12 2020.

[12] J. Piepmeier, P. Mohammed, G. De, A. E. Kim, J. Peng, and C. Ruf, "Soil moisture active passive (smap) algorithm theoretical basis document (atbd) smap calibrated, time-ordered brightness temperatures l1b$_t bdataproduct,''$ 2014.